Design and Synthesis of Air-Stable *p*-channel Conjugated Polymers for High Signal-to-Drift Nitrogen Dioxide and Ammonia Sensing

Tushita Mukhopadhyaya, Justine S. Wagner, Huidong Fan and Howard E. Katz*

Department of Materials Science and Engineering and Department of Chemistry, Johns Hopkins University, 206 Maryland Hall, 3400 North Charles Street, Baltimore, MD 21218, United States

*corresponding author: email hekatz@jhu.edu

Abstract

The development of high-performance conjugated polymer-based gas sensors involves detailed structural tailoring such that high sensitivities are achieved without compromising the stability of the fabricated devices. In this work, we systematically developed a series of diketopyrrolopyrrole (**DPP**)-based polymer semiconductors by modifying the polymer backbone to achieve and rationalize enhancements in gas sensitivities and electronic stability in air. NO_2 and NH_3-responsive polymer-based organic field-effect transistors (**OFET**s) are described with improved air stability compared to all-thiophene conjugated polymers. Five **DPP**-fluorene based polymers were synthesized and compared to two control polymers and used as active layers to detect a concentration of NO_2 at least as low as 0.5 ppm. The hypothesis that the less electron-donating fluorene main chain subunit would lead to increased signal/drift compared to thiophene and carbazole subunits was tested. The sensitivities exhibited a bias-voltage dependent behavior. The proportional on-current change of **OFET**s using a dithienyl **DPP**-fluorene polymer reached ~614% for an exposure to 20 ppm of NO_2 for 5 minutes, testing at a bias voltage of -33 V, among the higher reported NO_2 sensitivities for conjugated polymers. Electronic and morphological studies reveal that introduction of the fluorene unit in the **DPP** backbone decreases the ease of backbone oxidation and induces traps in the thin films. The combination of thin film morphology and oxidation potentials governs the gas-absorbing properties of these materials. The ratio of responses on exposure to NO_2 and NH_3 compared to drifts while taking the device through repeated gate voltage sweeps is the highest for two polymers incorporating electron-donating linkers connecting the **DPP** and thiophene units in the backbone, in this category of organic semiconductors. The responses to NO_2 were much larger than that to NH_3, indicating increased susceptibility to oxidizing vs reducing gases, and that the capability of oxidizing gases to induce additional charge density has a more dramatic electronic effect than when reducing gases create traps. This work demonstrates the capability of achieving improved stability with the retention of high sensitivity in conjugated polymer-based **OFET** sensors by modulating redox and morphological properties of polymer semiconductors by structural control.

Keywords signal-to-noise, gas sensing, air stability, electrical stability, diketopyrrolopyrrole, nitrogen dioxide, free volume, drift

1. Introduction

NO_2 is a toxic gas, mainly released by the emissions of fossil fuel combustion, that can induce acute harm such as pulmonary edema and respiratory disorders even under exposure to ~1 ppm.[1,2] NH_3 is also highly toxic and corrosive, has a flammability range of 15-28% by volume and is irritating to the respiratory system, skin and eyes despite its widespread applications in refrigeration and manufacturing systems such as dyes, drugs, synthetic fibres, plastics, etc.[3] Because of the increasing attention to environmental issues in recent years and the known environmental toxicity of NO_2 and NH_3, it is highly desirable to design and fabricate long-term-reliable, highly-sensitive, miniaturized, room-temperature-operating and low-power-consuming gas sensors, which can enable the real-time detection and sensing of these vapors. Although inorganic metal oxides as active materials are more stable than organic field effect transistor **(OFET)** sensors, they suffer from drawbacks such as limited selectivity and high operational temperatures which restricts their applications.[4,5] Recently, gold decorated carbon nanotubes[6], graphene[7] and aminoanthroquinone-modified graphene[8] have been explored as potential semiconducting materials for sensing applications because of ultralow detection limits (~0.6 ppb) of NO_2. Organic thin film transistors (**OTFT**s) employing Cu nanowire devices[9,10] and cobalt phthalocyanine have been shown to be strong reversible receptors for NH_3 and NO_2 gases.[11] However, **OFET**s built from conjugated polymers and oligomeric materials have also gained increasing attention as gas sensors because of certain advantages such as low cost, light weight, and ease of large-scale fabrication, which is made possible by facile solution and printing processability.[12,13] Conjugated polymers also allow broad diversity and structural tuning by the virtue of variability in molecular design by incorporating specific functional groups or by modulating the backbone oxidation potential to impart the recognition capabilities to target analytes by employing the appropriate device configuration or geometry.[14] For example, flexible gas sensors based on **DPP**-selenophene based polymers have been demonstrated to exhibit high and reliable NH_3 gas sensing with high ambient and bending stabilities with a 100 fold increase in channel resistance.[15] A highly sensitive printed NH_3 gas sensor with fluorinated difluorobenzothiadiazole-dithienosilole polymer (**PDFDT**) has also been reported which detected NH_3 down to 1 ppm with high sensitivity ~56%.[16] Efficient NH_3 sensing in PBTTT and thiophene-isoindigo donor-acceptor polymers was demonstrated

by controlling the cohesive interaction energies between the dielectric layer surface and the semiconductor layer, and the semicrystalline morphologies respectively[17,18] In a **DPP**-based conjugated polymer functionalized with t-boc groups, a dramatic and selective change in the hole mobility was observed after treating the **FET** with 100 ppb ammonia.[19] Ultra-sensitive nitrogen dioxide (NO_2) gas sensors based on 6,13-bis(triisopropylsilylethynyl)pentacene (TIPS-pentacene) **OTFT**s are reported with limit of detection (LOD)=1.93 ppb by balancing the crystallinity and grain density in **TIPS**-pentacene films. Chi *et al.* demonstrated an ultrasensitive NO_2 gas sensor based on 6,13-bis(triisopropylsilylethynyl)pentacene (TIPS-pentacene) which exhibits an ultrahigh sensitivity of more than 1000% ppm^{-1} at several ppm, a fast recovery time, and a calculated LOD of 20 ppb. [20,21] TIPS-pentacene films exhibited a porous morphology which allows gas molecules to easily penetrate into the channel region, thereby improving the gas sensing properties by ~20% for very low exposure times ~5s.[22] Apart from polymer functionalization and structural tailoring, using composite materials or employing polymer blends is also an important strategy to enhance the sensitivity of NO_2 sensors because of the larger ratio of surface area to volume, especially for polythiophenes.[23,24] Self-assembling monolayer field-effect transistors (**SAMFET**s) have also gained popularity due to their low detection limit, because of the enhancement of specific interactions with a target analyte on top of the semiconductor.[25]

However, **OFET** sensors possess inherent drawbacks such as the lack of air stability due to the susceptibility of the sensing functionalities to reaction with moisture and oxygen under ambient conditions, lack of selectivity, and a baseline drift problem which limits their range of application in organic circuits.[26,27,28] On exposure of polymers to oxygen and light, current and threshold voltage stabilities are lowered due to free radical reactions, and photo-oxidation occurs resulting in the formation of deep traps.[29] Although regioregular polyhexylthiophene (P3HT) was reported as an active layer to detect NO_2, it lacks selectivity.[30,31,32] Therefore, the development of simple, selective and high-performance detectors sensing NO_2 and NH_3 concentrations in the 1−10 ppm range remains a challenge and needs further development. For unencapsulated OFETs, the bias stress effect (**BSE**)-induced threshold voltage shift under continuous bias during operation leads to the trapping of charge carriers into less mobile localized states which is accelerated by oxygen and water.[33] To date, some approaches to reduce or passivate these trap sites include the use of post processing thermal annealing or by employing the

self-assembled monolayer (**SAM**) technique.[34,35] Oxidative degradation of the dielectric layer films under ambient conditions can also cause device degradation.[36,37] Morphological effects such as bulk defects or porosities in the thin film are also reasons behind V_{th} instabilities in **OFET**s. In the past, several air-stable organic semiconductors have been developed by either modifying the side chains or by employing functional groups less susceptible to aerial oxidation. Recently, attempts have been made to develop air-stable conjugated polymers for gas sensors by using benzodithiophene derivatives and P3HT using a double-layer strategy.[38] Also, polymer derivatives of organosilicon derivative of [1]benzothieno[3,2-b][1]-benzothiophene have been reported exhibiting air stability and high sensitivity with regards to detection of H_2S and NH_3 at concentrations ~200 ppb.[39] *However, no prior study has compared vapor sensitivities to current or voltage drifts over comparable times, nor separated the molecular-scale morphological, environmental, and bias stress contributions to those drifts.*

In this work, we have designed and synthesized five **DPP**-fluorene based donor-acceptor copolymers by introducing structural variations to a moderately electron donating, and therefore stabilizing, main-chain fluorene unit covalently linked to the **DPP**-unit so as to (i)modify the backbone conformation (ii) modify the backbone oxidation potential and (iii) tailor the thin film morphology to modulate the gas sensing properties.

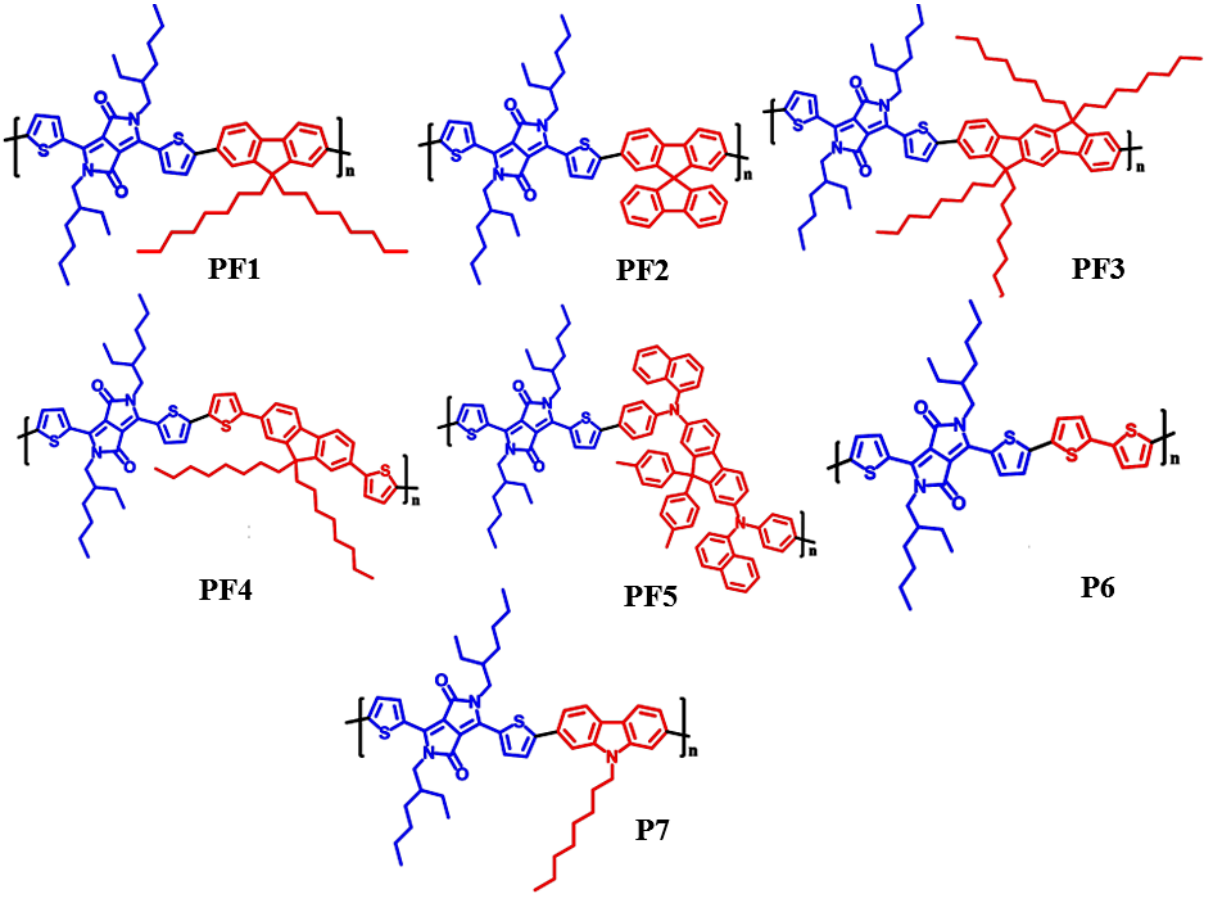

Figure 1. Molecules of Interest

The incorporation such main-chain groups not only increases the polymers' conformational flexibility and entropy but also allows mutual rotation of adjacent side chain elements about the flexible moieties. At the same time, changing the nature of these main chain groups allow for the modulation of the geometry of the otherwise rigid chain.[40,41] The responses to NO_2 and NH_3 of the five **DPP**-fluorene based polymers (**PF1-PF5**) were compared to that of control commercial polymers **P6,** lacking the fluorene unit and **P7,** incorporating an electron-donating carbazole unit instead of the fluorene unit, respectively. The structures of the polymers are shown in **Figure 1**. The relative contributions of backbone electronic structure and microstructure in sensing of NO_2 and NH_3 gases were thoroughly explored.

Cyclic voltammetry measurements revealed that introduction of the fluorene unit in the **DPP** backbone makes the frontier energy levels more positive relative to a standard potential, and morphological studies confirm that modification of the spacer fluorene group leads to varying morphologies in thin films that affect the vapor response. We observed that the ratio of responses on exposure to NO_2 and NH_3 / drifts taking the device through repeated gate voltage sweeps is the highest for the polymer incorporating an

electron-donor linker between the **DPP** and the fluorene derivative among this set of semiconductors. The responses to NO_2 were much larger than that to NH_3, indicating different susceptibility to oxidizing and reducing gases. This work demonstrates the capability of achieving improved stability with the retention of high sensitivity of conjugated polymer-based **OFET** sensors by modulating redox and morphological properties of polymer semiconductors.

2. Results and Discussion

2.1 Synthesis and Characterization

The synthetic scheme for the five polymers is shown in **Figure S1, SI**. The polymers where **DPP** is coupled to dithiophene and carbazole were obtained commercially. The polymers have been named **PF1**, **PF2**, **PF3**, **PF4**, **PF5**, **P6** and **P7**. The polymers were synthesized by a C-H activation reaction involving appropriate monomers having the dibromo- functionality in the presence of $Pd(OAc)_2$ with pivalic acid as the active ligand.[42] The crude polymers were taken through a series of three precipitations in methanol and further purified through Soxhlet extraction in hot methanol, acetone and hexane to remove unreacted starting materials, monomers and shorter oligomers and catalytic impurities. Post soxhlet purification, the polymers were precipitated again from chloroform solution into methanol and the residue collected by vacuum filtration. The **DPP** monomers were functionalized with the branched 2-ethylhexyl side-chain to induce solubility in common organic solvents for easy thin-film processing. Structural characterization of the monomers was carried out using ^1H NMR and Gel Permeation Chromatography (**GPC**) (**Figures S1-S12, SI**). The molecular weights and **PDI** were evaluated by **GPC** and are shown in **Figure S7-S12** and collected in **Table S1, SI**.

2.2 Optical, Electrochemical and Thermal Properties

The steady-state optical properties of the polymers **PF1-PF5** and **P6** were studied using UV-visible spectroscopy (**Figure 2**). The structural changes introduced into the polymer backbone by varying the nature of the fluorene group in the **DPP**-fluorene based polymers are reflected in the backbone planarity and aggregation properties in solution and in the solid state. The measured parameters from the UV-visible spectra and the electrochemical data (**Figure S13)** are collected in **Table 1**.

Table 1. Summary of Optical and Electrochemical properties of **DPP**-fluorene based polymers

Polymers	λ_{max}, solution (nm)	λ_{max}, film (nm)	E_g(opt)(eV)	HOMO (CV)(eV)
PF1	644.5	655.9	1.35	-5.37
PF2	643.1	654.5	1.36	-5.47
PF3	644.5	653.4	1.38	-5.29
PF4	664.8	684.6	1.34	-5.19
PF5	648.9	657.5	1.37	-5.18
P6	777.3	767.1	1.30	-5.12
P7	672.1	699.9	1.63	-5.24

The thin-film spectra of all polymers exhibited a bathochromic shift compared to the solution-phase spectra, which is consistent with the increase in intermolecular interaction and aggregation in thin films compared to solution. The copolymers showed

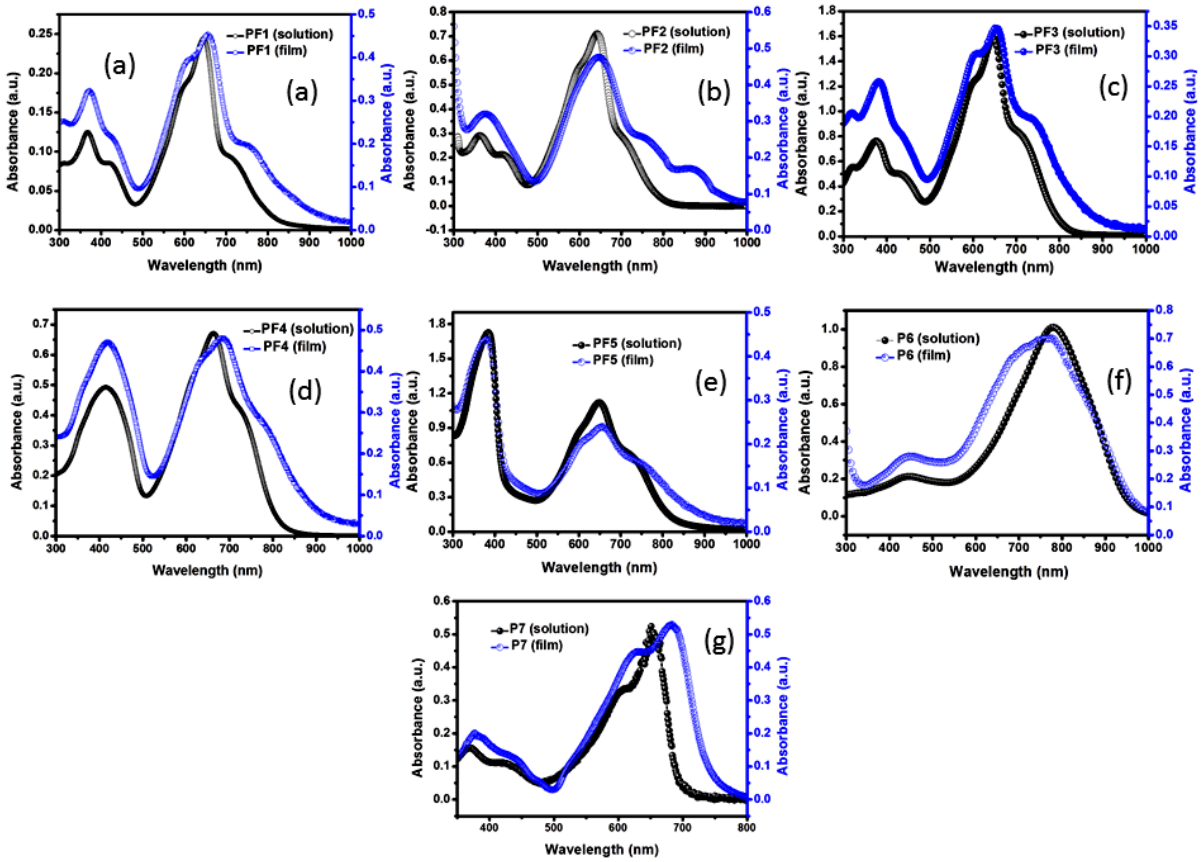

Figure 2. UV-visible spectra of (a)**PF1** (b)**PF2** (c) **PF3** (d) **PF4** (e) **PF5** (f) **P6** and (g) **P7** in solution and thin films

a strong shoulder at ~370 nm which corresponds to the π-π* transition of the fluorene moiety.[42][43] All polymers exhibit well-resolved vibrational structure with two maxima between 600- and 700 nm. For **PF3**, **PF4** and **PF5**; the intensity of the lowest energy peak is observed to become more prominent (amongst the fluorene-containing polymer series) which is consistent with increasing backbone planarity and resulting aggregation of the polymer chains compared to **PF1** and **PF2**. On comparison of the solution-phase absorption maxima (λ_{max}) of the fluorene-containing polymers, we found that **PF4**> **PF5**> **PF3**~**PF1**>**PF2**. **PF4** has additional thiophene linkers which increase backbone donor strength and maximizes donor-acceptor interactions and also helps overcome the ortho hydrogen repulsions. This explains the red-shifted solution-phase absorption spectra of

PF4 compared to their counterparts **PF3**, **PF1** and **PF2** in which the **DPP** unit is coupled to the fluorene unit by single thiophene rings. Although the absorption maxima of **PF1** and **PF3** are situated at similar wavelengths, the very slight red shift and the relatively higher intensity of the higher wavelength peak is because the fused indeno[1,2-b]fluorene (**IDF**) unit provides extended π−π conjugation facilitating intermolecular interactions thereby reducing the rotational disorder around interannular single bonds. The fluorene unit with the bridgehead sp^3 carbon with long alkyl chain substitution (**PF1**) and spiro substitution (**PF2**) impair effective π-π stacking and inhibit the close packing of the polymer chains polymers leading to a blue-shifting of the spectra. We observe that despite their bulkiness and conjugation- interrupting nature, the inclusion of the spirofluorenyl and triarylamino groups do not appear to change the thin film aggregation as is evident from the high-wavelength portion of the UV-visible spectra. [44]

P6 exhibits the highest λ_{max} amongst all polymers in this series due to removal of the backbone torsional defect as a consequence of the absence of the fluorene unit; leading to enhanced intermolecular interaction and high degree of planarity and π-π stacking. The optical gap of **P7** is larger, ~1.6 eV. [45]

The effects of structural modifications on the oxidation potential (**HOMO**) of the polymers were evaluated by cyclic voltammetry of the polymers in solution. Pt was used as the working electrode and Ag/AgCl as the reference electrode in 0.1 M tetrabutylammonium tetrafluoroborate acetonitrile solution with a scan rate of 0.5 V s^{-1} and the tests were calibrated using a ferrocene/ferrocenium redox couple. The cyclic

voltammograms are shown in **Figure 3**. **PF1, PF3, PF4 and PF5** show quasi-reversible two-electron oxidation cycles; indicates the participation of the fluorene and thiophene donor chromophores in the oxidation process. **P6** shows a one-electron reversible oxidation cycle. This corroborates with our observations from the UV-visible studies that there is greater delocalization of the **HOMO** levels in **P6** rendering it more favorable to become oxidized. The **HOMO** levels extracted from the onsets of the oxidation waves in the **CV** data are shown

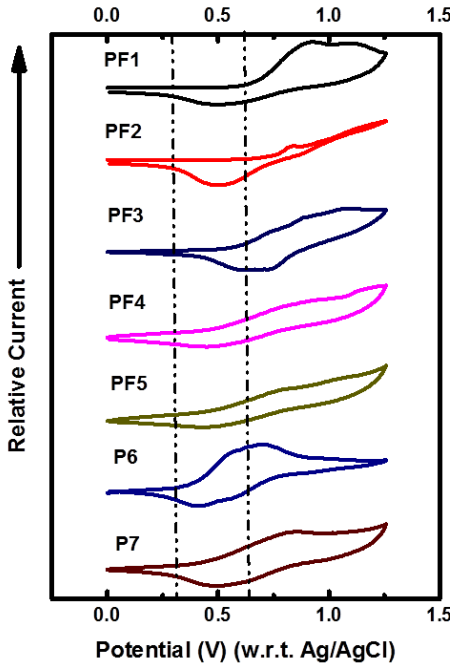

Figure 3. Cyclic voltammograms (oxidation window) at scan rates of 0.5Vs^{-1} for **PF1-PF5** and **P6** and **P7** films on glassy carbon.

in **Table 1**, which reveal that the polymers with a higher degree of backbone planarity (evident from larger bathochromic shifts) also possess lower oxidation potentials, rendering them easier to oxidize. Thus, the **HOMO** levels of **PF1**, **PF2** and **PF3** are deeper compared to those of **PF4**, **PF5** and **P6** and **P7**. Stronger electron donors such as bithiophene and carbazole are responsible for the elevation of **HOMO** levels. The CV of the reference compound ferrocene is shown in **Figure S13, SI**.

Thermal properties of the polymers were evaluated by differential scanning calorimetry (**DSC**) measurements. The **DSC** plots are shown in **Figure S14, SI**. The **DSC** curves show that **PF1**, **PF2**, **PF3**, **PF4**, **PF5** and **P6** exhibit broad, endothermic peaks at 149.0°C, 148.75°C, 145.6°C, 157.8°C, 154.4°C, 159.9°C and 131°C respectively,

corresponding to the glass transition temperatures of the polymers. We have estimated the percentage free volume at a given temperature of the polymers from the **DSC** measurements using the equation: $\mathbf{(V_{free:exs,\ SB}/V) \approx (\alpha_L - \alpha_G)T}$ where α is the coefficient of thermal expansion in the liquid(**L**) and glassy (**G**) states, and $V_{free:exs,\ SB}/V$ quantifies the fraction of free volume belonging to segments behaving in a solid-like manner.[46] Larger free volumes are associated with more chain ends per volume. Since $(\alpha_L - \alpha_G) \sim 0.113/T_g$ the percentage free volumes can be estimated as: 9.10%, 9.12%, 9.33%, 8.50%, 8.75% , 8.51% and 10.43% respectively at the device annealing temperature of 120°C used for the sensor **OFET**s. We hence observe that **PF1, PF2**, **PF3** and **P7** have higher free volumes due to larger numbers of side-chains per unit volume. **PF4** and **PF5** possess linkers that decrease the number of side chains per unit volume by increasing the distance between the side chain-bearing units. For a given diffusant, the diffusivity is a decreasing linear function of $1/(V_{free:exs,\ SB}/V)$ as predicted by the free volume theory. It has also been observed that $\log_{10}$ [diffusivity]=A'-B'/FFV, where B is the "jumping unit", which decreases with increasing chain stiffness, implying that gas molecules should diffuse faster in stiffer polymers than flexible ones with same fractional volume.[47]

2.3. Device measurements

OFETs were fabricated in the top-contact, bottom-gate architecture as sensing devices. The polymer semiconductors were spin-coated from a 10 mg mL^{-1} chloroform solution at 2000 rpm and annealed at 120 °C for 20 min in the glovebox. The film thicknesses were measured as 70±15 nm, 90±5 nm, 105±25 nm, 80±9 nm, 84±10 nm, 125±13 nm, 113±5 nm for **PF1-PF5**, **P6** and **P7** respectively (**Figure S20**, **SI**). The difference in thickness arises due to solubility and viscosity. Au source/drain electrodes (W =1.1 cm, L = 200 μm) were used to measure the electrical performances of the polymer-based devices. The field-effect mobilities were calculated from the transfer characteristics of six devices in the saturation region. The original devices without gas exposure show typical *p*-type transport. The output curves and transfer curves are shown in **Figures S15 and S16, SI** respectively. The hole mobilities and the threshold voltages (V_{th}) of the transistors are collected in **Table S2, SI**. **P6** shows a high hole mobility of 0.12± 0.02 $cm^2V^{-1}s^{-1}$and **P7** shows a hole mobility of $(3.1x10^{-3}) \pm (3\ x10^{-4})$ $cm^2V^{-1}s^{-1}$. **P3** shows hole mobility of $\sim (1.2x10^{-3}) \pm (7x10^{-4})$ $cm^2V^{-1}s^{-1}$ while films of the other four polymers exhibit much lower hole mobilities $\sim 2.0x10^{-4}$ $cm^2V^{-1}s^{-1}$, though mobility will

not be the only determining factor in response and stability parameters discussed below. Note that the V_{th} values (**Table S2, SI**) of the polymers containing the fluorene spacer are higher than those of **P6** and **P7**. The trends in mobilities (**Table S2, SI**) are consistent with the UV-visible studies and **CV** which predict that a greater effective conjugation length implies good π-π stacking with consequently low thin-film defect densities leading to higher hole mobilities.

All polymers except the lower-mobility polymers **PF4** and **PF5** show substantial hysteresis in the transfer characteristics which is probably due to trapped charges in the semiconductor bulk or interface, or polaron/bipolaron interconversion due to the charged states of the polymer depending on the direction of the gate sweep.[48]

The morphology of the polymer films was studied by atomic force microscopy (**AFM**) in the tapping mode (**Figure S17, SI**). Films of polymers **PF3**, **PF4**, **P6 and P7** exhibit more continuous grains and better coverage which reflects in their low root mean square roughnesses (r.m.s.) of 0.56 nm, 2.74 nm, 1.72 nm and 2.54 nm respectively; which aids charge transport. **PF1**, **PF2, PF3** and **PF5** exhibit lesser surface coverage and smaller grains connecting the grains and possess r.m.s. roughness of 4.25 nm, 6.79 nm, 0.562 nm and 5.88 nm respectively. A smoother film surface topology is associated with lesser traps and grain boundaries and hence, higher *p*-channel mobilities.

The procedures and results of the stability measurements of devices fabricated from **PF1-PF5, P6** and **P7** are as follows. Immediately post-fabrication, the transfer curves were recorded on day 1. The devices were then subjected to repeated gate sweeps for 25 cycles at a constant rate of 0.5 Vs^{-1} (**Figure S18, SI**) on day 2, to separately observe one day's worth of environmental drift from drift induced by bias stress. The devices were **then** stored in ambient air for 24 hours and the transfer curves were recorded again on day 3 to record the extent of recovery and compared (overlaid) with the transfer curve on day 1. The devices were then exposed to ambient air for a period of 45 days and the transfer curves recorded again and compared to the immediate transfer curves post-fabrication (day 1). We monitored the source-drain current at the highest gate voltage V_G=-100 V for reference (**Figure S19, SI**). The conclusion from **Figure S19** is collected in **Figure 4**. The deviations from the original current (post fabrication) after applying dynamic bias stress and air exposure are indicators of the stability of the devices, particularly for the 45-day storage condition. Polymer **P6** recovers particularly quickly

and completely from bias stress, as shown by the "day 3" point of **Figure 4** relative to the very large bias stress effect shown in **Figure S18, SI.**

The currents show a decreasing trend with an increase in the storage time irrespective of the electronic structure of the polymer. The microscopic device degradation mechanism under bias stress (repeated gate sweeps) arises from threshold voltage shifts after bias stress which results from slow trapping of charge carriers and is often accelerated by exposure to water and oxygen in the atmosphere.[49]

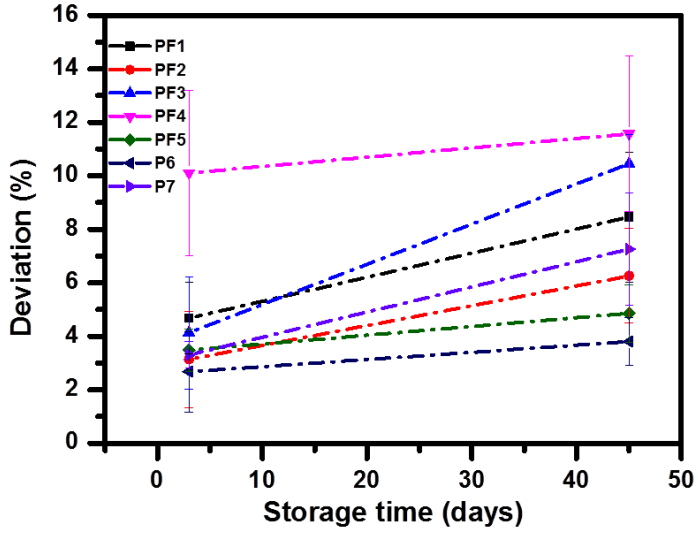

Figure 4. Stability measurements of **OFET**s as a function of storage times (days) based on **PF1-PF5**, **P6** and **P7**. Deviations (%) are calculated as $(I_{day\ 1}-I_{day\ 3})/I_{day1}$ and $(I_{day\ 1}-I_{day\ 45})/I_{day1}$

As mentioned before, the **OFETs** fabricated from the polymers were subjected to continuous gate sweeps and the approach to final transfer current was fit to the relationship $I_t\ \alpha\ \exp(-t/\tau)$[50] or a first order Arrhenius rate equation in the logarithmic form $\ln I_t = \ln I_0 - kt$. The voltage sweeps were carried out at ~0.5Vs^{-1} for 25 cycles (**Figure S21, SI**). The rate constants for the process were ~10^{-4} s^{-1} for all the polymers in the series except for **PF4, PF5** and **P7** (~10^{-5} s^{-1}) with additional heteroatoms besides the single fluorene-connecting thiophenes. Charge carrier traps are formed in the grains while surrounding grain boundaries act as insulating barriers for trapped charge preventing them from crossing the grain boundaries.[51] The additional electron-donating linkers in **PF4, PF5** and **P7** may inhibit or undergo transformation competitive with trap formation, slowing the formation of the final trap density by gate bias.

To measure responses to a given NO_2 and NH_3 concentration, we prepared 6 sensing devices from each polymer for each gas exposure experiment. The vapors were diluted by air that has the same humidity and components as the ambient atmosphere. The devices were subjected to repeated gate voltage sweeps (~25 cycles) to allow the devices to stabilize before exposure to NO_2 and NH_3 vapors. Sensing devices were tested after exposure to NO_2 gas, i.e. **OFET**s were turned on after the period of NO_2 and NH_3 exposure ended. The **OFET**s showed significantly increased drain current when exposed to NO_2 gas while a decrease in current (I_{DS}) was observed on exposure to NH_3 gas. The transfer curves of optimized devices for NO_2 and NH_3 exposure are shown, up to -100 V, in **Figure S22** and **S23, SI** respectively. Change in drain current (ΔI_{DS}) was used as a measure of the sensitivity of these devices, calculated by the formula $100\% \times (I_{DS,NO2} - I_{DS,air})/I_{DS,air}$, where $I_{DS,NO2/NH3}$ is the drain current after exposure to NO_2 or NH_3, and $I_{DS,air}$ is the drain current before exposure to NO_2 or NH_3. We monitored the sensitivity at -80 V, -60 V and at (V_{th}-40) V for each polymer. 40 V is a typical range above V_{th} at which the transistor is on whilst the effects of shallow traps and contact resistance are minimized in comparing sensitivities.[52,53] *We also define a new response-to-stability parameter 'D' calculated as* $D= (\Delta I/I)_{exposure,\Delta t}/(\Delta I/I)_{without\ exposure,\Delta t}$ *where Δt is the time interval of exposure of the sensing device to the vapors for a particular concentration of the gas.* The last five cycles out of twenty-five, each taking about 1 minute and after most bias stress and device burn-in had occurred, were used to measure a *five minute drift before a five minute exposure* to analyte vapor was used to determine sensitivity for calculating the 'D' values. These percentage drifts are collected in **Table 2**. The reason for lesser drift in **PF4** and **PF5** is presumably related to the apparent slower trapping processes and lower hysteresis in those polymers discussed above. **PF4** and **PF5** are characterized by relatively low free volume and a seemingly optimal oxidizability, less facile than **P6** and easier than the others. *Note that these percentage drifts are the ones that would be most related to the "noise" relative to signals from exposures to* NO_2 *and* NH_3.

Table 2. Percentage drifts at -80V, -60V and at V'=V_{th}-40 V

Polymers	**$(\Delta I/I)_{-80V}$ (%) (5mins)**	**$(\Delta I/I)_{-60V}$ (%) (5 mins)**	**$(\Delta I/I)_{Vth-40}$ (%) (5 mins)**
PF1	6.7±2.4	9.7±5.4	17.8±10.6
PF2	7.8±4.8	16.1±4.8	21.2±2.9
PF3	9.2±6.5	12.6±8.2	21.4±2.7

PF4	2.1±1.7	2.5±1.4	4.4±4.4
PF5	1.9±1.4	1.5±0.9	4.4±2.5
P6	5.8±1.2	7.8±1.5	15.4±1.9
P7	4.9±2.1	7.5±4.2	10.5±5.9

The polymer **OFET**s show gate-voltage dependent responses using the same voltages for all seven polymers. The percentage responses at each of the concentrations are quantified in **Figure 5** and **Figure 6** for NO_2 and NH_3 respectively. We show the responses for 1, 5, 10 and 20 ppm of NO_2 and NH_3 on exposing the devices to each concentration of the gases for 5 minutes. The fixed voltages were chosen so all the **OFETs** were well in accumulation to avoid the noise at the near-threshold voltage region. We also studied the sensitivities at -40 V (into the accumulation regime) vs. the threshold voltage of each polymer **PF1** to **P7** to evaluate the relative contributions of the variables such as oxidation potential, morphology, free volume and conformational flexibility to the gas-sensing properties *under the fairest practical conditions* as mentioned above. Both the NO_2 and NH_3 sensors are endowed with much higher sensitivity under lower gate voltages on exposure to both the gases.

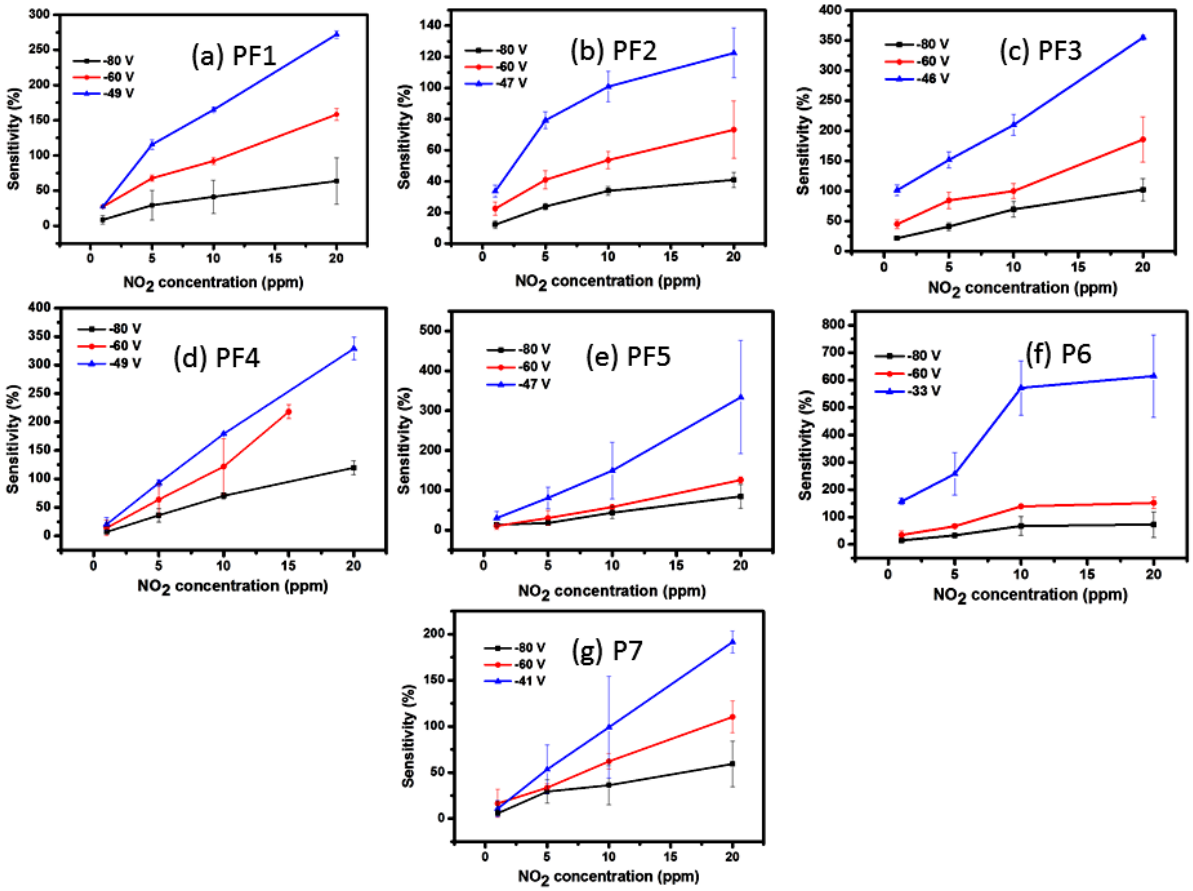

Figure 5. Sensitivity of polymers (a) **PF1** (b) **PF2** (c) **PF3** (d) **PF4** (e) **PF5** (f) **P6** and (g) **P7**, on exposure to NO_2 gas (1, 5, 10 and 20 ppm) for 5 minutes. The sensitivities were calculated at -80 V, -60 V and V= (V_{th}-40)

With gate voltage of −60 V, the sensors based on **PF2** films exhibit the least sensitivity, up to ~22% and ~73% under 1 ppm for 5 min and 20 ppm for 5 min, respectively. As discussed earlier, **PF2** has a non-planar backbone and low backbone electron density. On the other hand, the proportional on-current change of **OFETs** using the most easily oxidizable **P6** reached ~157% for 1 ppm, 256% for 5 ppm, ~570% for 10 ppm and ~614% for an exposure to 20 ppm of NO_2 for 5 minutes at a bias voltage of -40 V fully in accumulation for the polymer. The responses of the other five polymers are of the same order of magnitude.

We tabulated the sensitivities with V_G set to (V_{th}-40) in **Tables 3** and **4** to show the trends in NO_2 sensitivities. Response to high NO_2 concentration (**PF3, PF4, PF5,** and **P6**, 20 ppm) seems to correlate with ease of *p*-doping driven by a large driving force for electron transfer from the **HOMO** of the polymer and the **LUMO** of NO_2 gas.[55,56] Responses to lower concentrations (1-10 ppm) of NO_2 exposure appear to be enhanced by increased

free volume for polymers **P1** and **P3.** Polymer **P7** seems surprisingly unresponsive to NO_2 considering both of these properties.

Meanwhile, the sensors based on **PF1-PF4, P6 and P7** show responses of 20-30% respectively to NH_3 at -60 V, while the sensitivities were ~30-40% in the (V_{th}-40) regime, on exposure 20 ppm NH_3 for 5 mins (**Figure 5**). **PF5** however exhibits a response of ~56% at -60 V and ~67% in the (V_{th}-40) regime. To the extent that this difference might be significant, we propose the involvement of the lone pair of electrons on the bridging nitrogen atom of **PF5** with hydrogen bonding interactions with NH_3, facilitating chemically induced trap formation. Otherwise, the polymers exhibit similarly lower responses to NH_3, irrespective of the backbone electronic structure and morphology/free volume, than those to NO_2.

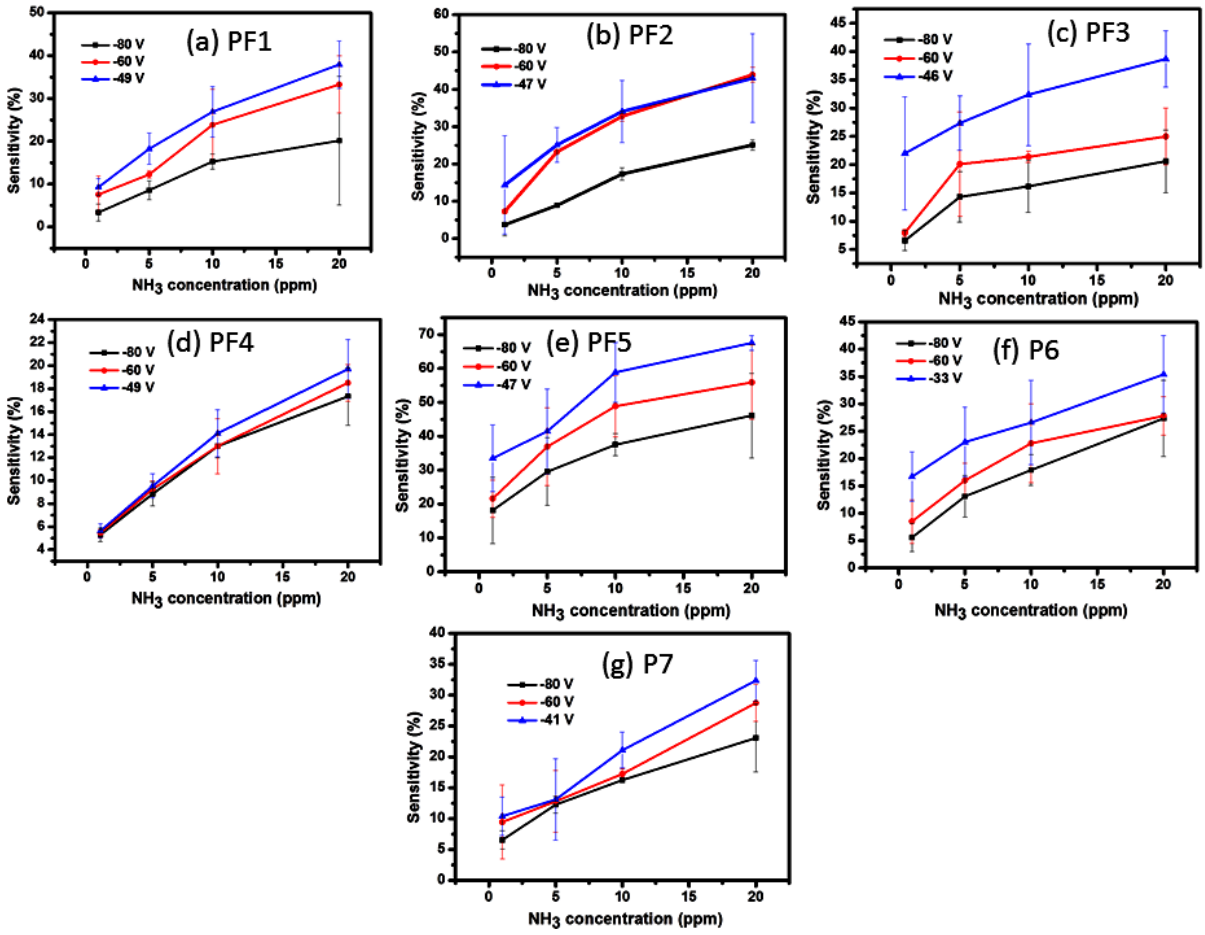

Figure 6. Sensitivity of polymers (a) **PF1** (b) **PF2** (c) **PF3** (d) **PF4** (e) **PF5** (f) **P6** and (g) **P7** on exposure to NH_3 gas (1, 5, 10 and 20 ppm) for 5 minutes. The sensitivities were calculated at -80 V, -60 V and V= (V_{th}-40) V.

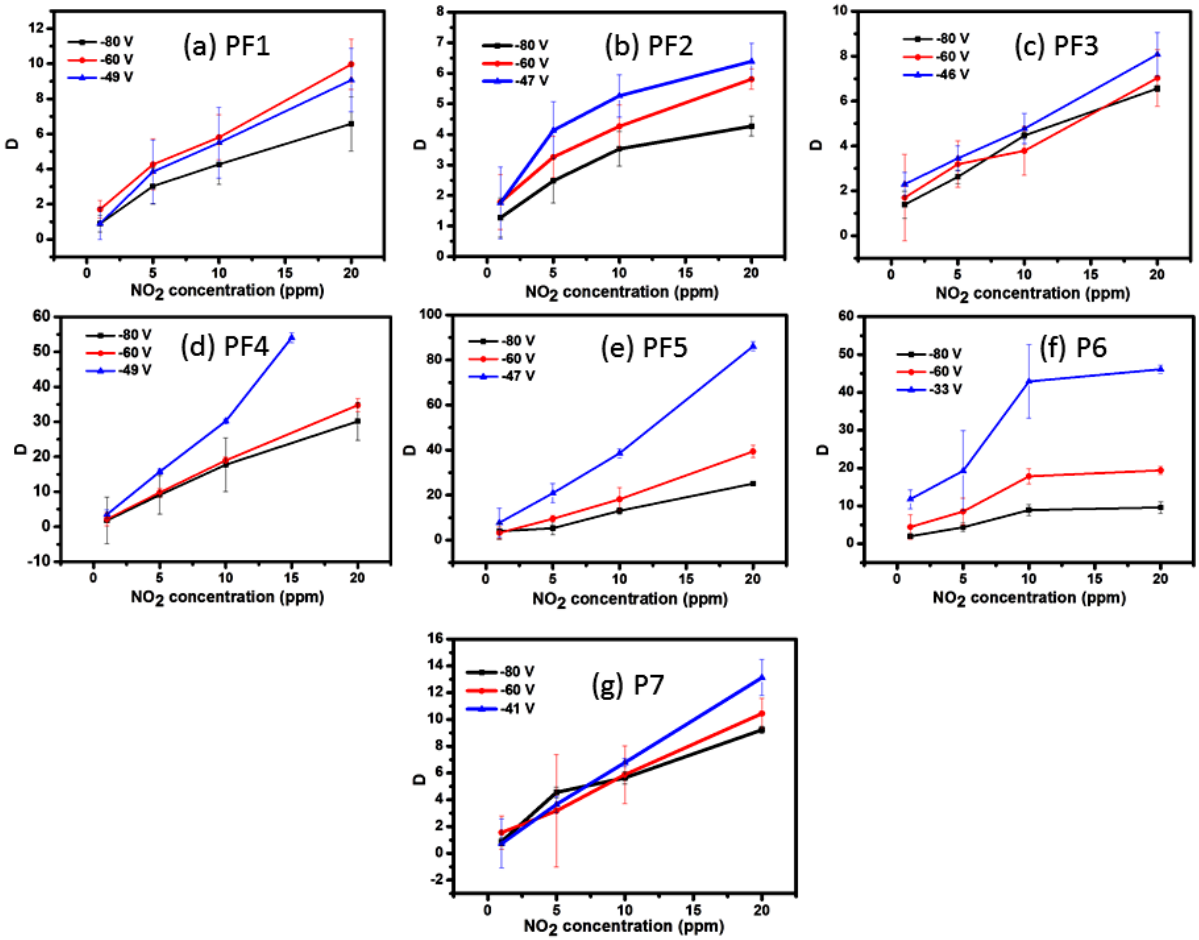

Figure 7. 'D' values of polymers (a) **PF1** (b) **PF2** (c) **PF3** (d) **PF4** (e) **PF5** (f) **P6** and (g) **P7** on exposure to NO_2 gas (1, 5, 10 and 20 ppm) for 5 minutes. The sensitivities were calculated at -80 V, -60 V and V= (V_{th}-40) V.

The D values (defined above) for NO_2 sensitivity, plotted in ***Figure 7*** *and listed in* ***Table 3****, are the highest for* ***PF4*** *and* ***PF5*** *due to their low drifts and for* ***P6*** *by virtue of its high sensitivity despite the drifts.* All of these have relatively electron donating linker subunits, but different degrees of conjugation that apparently influence the relative importance of high sensitivity versus low drift. It is interesting to note that **PF1**, **PF2**, **PF3** and **P7** exhibit similar D values (~6-9) despite different responses, which reveals that in those cases the drift and response balance each other out. The resultant D values for NH_3 sensitivity are the highest for the least conjugated but most H-bondable **PF5** both by the virtue of its moderate sensitivity and low drifts **(Figure 8)**. Recall that the average percentage drifts in relative currents in the last five cycles of the devices at the gate voltage of interest with respect to measurements (before exposure to vapors) had been shown in **Table 2**. These

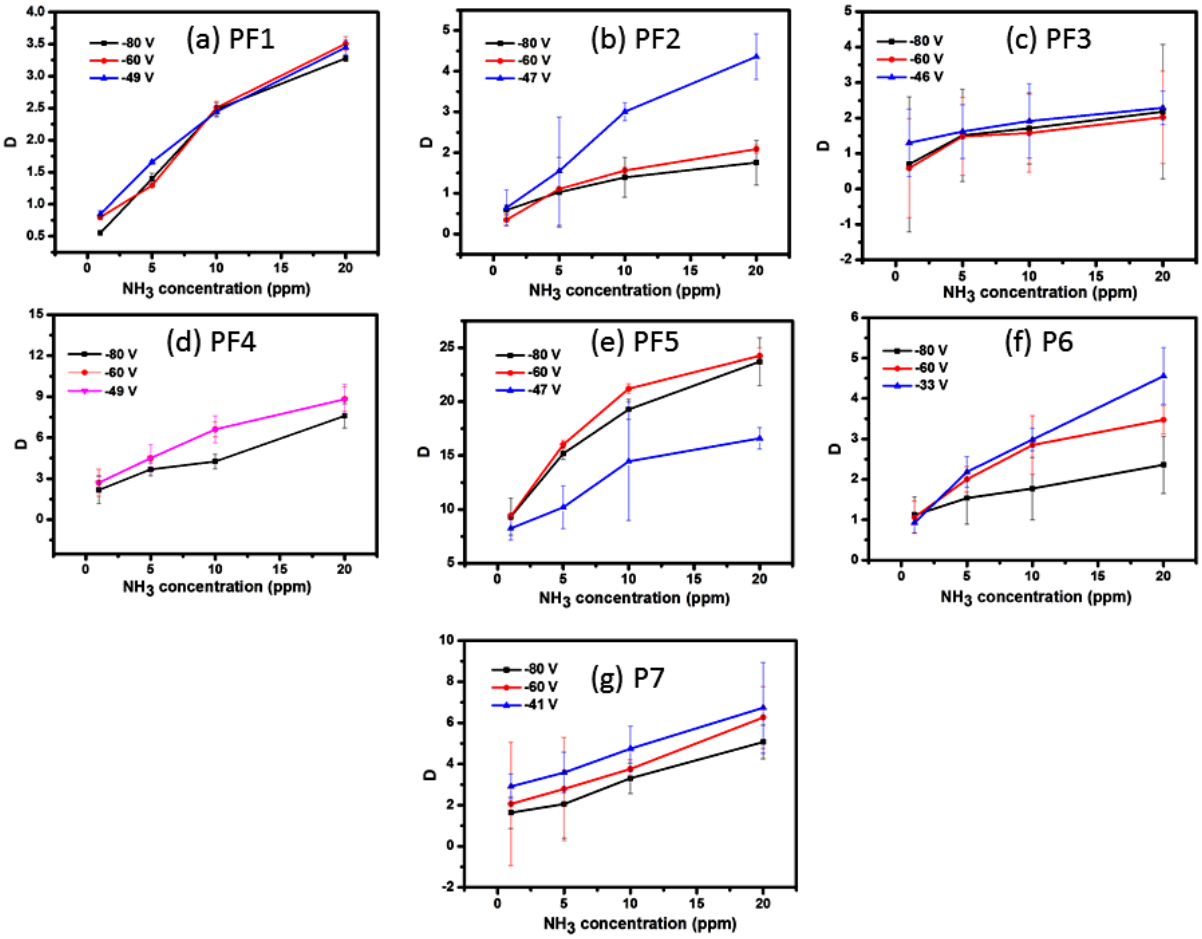

Figure 8. 'D' values of polymers (a) **PF1** (b) **PF2** (c) **PF3** (d) **PF4** (e) **PF5** (f) **P6** and (g) **P7** on exposure to NH_3 gas (1, 5, 10 and 20 ppm) for 5 minutes. The sensitivities were calculated at -80 V, -60 V and V'= (V_{th}-40) V

are the "drift" values used to calculate the parameter D. Note that the 'drifts' increase at lower gate voltages. The responses, drifts and the signal-to-noise ratios in the V_{th}-40 V regime for NO_2 and NH_3 sensing are collectively depicted in **Figure S24, SI**.

Table 3. NO_2 sensitivities and D values in the (V_{th}-40) regime

Polymer	Sensitivity (%) 1 ppm	Sensitivity (%) 5 ppm	Sensitivity (%) 10 ppm	Sensitivity (%) 20 ppm	D 1 ppm	D 5 ppm	D 10 ppm	D 20 ppm
PF1	27±0.7	115±6	165±4	272±5	1±1	4±1	5±2	9±2
PF2	34±4	79.2±5	101±9	122±15	2±6	4±4	5±2	6±2
PF3	10±9	152±13	210±17	355±4	2±3	3±1	5±1	8±2
PF4	20±12	93±6	179±1	329±20	2±1	10±1	19±2	35±1
PF5	30±17	81±27	150±15	334±9	8±1	21±1	39±2	86±2
P6	157±12	258±15	571±11	614±22	12±1	19±1	43±1	46±1
P7	10±9	53±18	99±25	192±12	1±1	4±2	7±1	13±1

Table 4. NH_3 sensitivities and D values in the (V_{th}-40) regime

Polymer	Sensitivity (%) 1 ppm	Sensitivity (%) 5 ppm	Sensitivity (%) 10 ppm	Sensitivity (%) 20 ppm	D 1 ppm	D 5 ppm	D 10 ppm	D 20 ppm
PF1	9±2	18±4	27±5	37±6	1±1	2±1	3±1	3±1
PF2	14±12	25±4	34±8	43±11	1±1	2±1	3±1	4±1
PF3	22±10	27±4	33±9	39±5	1 ±1	2±1	2±2	2±1
PF4	6±1	9±1	14±3	20±2	2±1	5±1	7±1	9±2
PF5	34±9	41±12	59±9	68±3	9±1	11±2	14±1	16±1
P6	16±4	24±6	27±7	36±8	1±2	2±2	3±1	5±1
P7	10±3	13±6	21±2	33±4	3±1	4±1	5±1	7±2

We also studied the kinetics of the recovery process after exposure to the gases. The plots of the $\log_e$ of the percentage recovery versus 1/T are shown in **Figures S25, SI**. After exposure to 20 ppm of gases for 5 minutes, the devices were kept in the vacuum oven at temperatures of 40^{o}C, 60^{o}C and 80^{o}C for three minutes at each temperature, and then removed for measuring the transfer curves to monitor the recovery process. On monitoring the percentage recovery of each of the polymers on subjecting the sensor to 40^{o}C for 3 minutes, we observe different rates of recovery (**Table S3, SI**), all pointing to fairly mild conditions for achieving reversibility, which is often sought in sensors. It happens that a device based on **P7** (which is the least responsive to NO_2 in the (V_{th}-40) regime) exhibits the highest activation energy and also a lower percentage recovery of ~24% compared to the other polymers; beyond that there is little if any association between the recovery kinetics and NO_2 sensitivities. Because the sensitivities include electronic effects from each molecular adsorption in addition to transport rates and interaction stabilities, they may not be strictly related to reversibility of responses, which only includes the latter two effects. We could not evaluate the activation energies of the

recovery process from NH_3 exposure as all devices almost completely recovered at 40°C within a time duration of 3 minutes. This does, however, indicate good reversibility.

Over time, polymer chains undergo relaxations via segmental motion towards a pseudo-equilibrium state of chain packing which decreases the free volume. As gas concentration increases, polymers swell and undergo free volume reorganization.[54] **P7** has the highest free volume as discussed previously, amongst all polymers in this series, which could lead to high free volume reorganization and therefore higher activation energy for desorption of analyte molecules.

The stability and response data vary considerably with the structures of the polymers and applied gate voltages. The highest NO_2 sensitivity, close to 600% at V_G=-33 V which is the first report of such high NO_2 response of a **DPP** polymer, seems to be associated with the electronic donating ability **P6** while the lowest drift from **PF4** and **PF5** was associated with lower free volume and moderate electron donating ability. This was also observed in an earlier study on PQT-12 and PQT-S12 from our group wherein PQT-S12 exhibited much higher sensitivity to NO_2 compared to PQT-12 consistent with PQT-S12 having slightly easier oxidizability; despite both having similar hole mobilities.[56] However, responses to several environmental solvents were higher from PQT-S12, and both of the PQT polymers, which are more electron-rich and much less stable than the polymers of this study, showed ~60-70% current output decreases on exposure of the devices to ambient conditions over several days.

Concluding remarks

A key figure of merit for these materials for their use in responsive devices is vapor response compared to instability on the same time scale as the measurement. Three polymers from the set studied in this work were identified as promising by this measure; two because of exceptionally low drift and a third being particularly sensitive to NO_2. A second figure of merit, for future consideration, is the vapor response differences in a pair of materials compared to drift differences. This second figure of merit determines the ability of a series circuit to produce a voltage output at the connection between the two devices that is selective for a vapor while the drift in the output voltage is minimized.[44]

With this in mind, the data show that **PF3** has substantial NO_2 response with fairly good stability parameters as well as fairly low oxidation potentials. **P7** has similar or better stability but generally less response to NO_2 tested at the same gate voltages. Thus, we anticipate that a series circuit with a voltage output taken at the connection from between devices with these two materials would be selective for NO_2 vapors, while the environmental stability would be considerably compensated.

Acknowledgments. This work was primarily supported by the National Science Foundation, ECCS Division, Award Number 1807293. Preliminary synthesis experiments and comparison with PQT-12 and PQT-S12 were supported by the Maryland Innovation Initiative (TEDCO). The participation of Huidong Fan (initial testing of polymer semiconductor performances) was funded by the China Scholarship Council. We thank Professor Patricia McGuiggan for assistance with AFM measurements. We also thank Garvin Peters and Yuyang Ji for their assistance in CV and GPC measurements using the facilities in Prof. J.D. Tovar and Prof. Rebekka Klausen's laboratories respectively.
We acknowledge insightful discussions with Professor Wudyalew Wondmagegn of the College of New Jersey.

Associated Content

Supporting Information

The Supporting Information is available free of charge on the ACS Publications Website at DOI.

Detailed methods, synthetic procedures, polymer characterization results from ^1H NMR spectroscopy and Gel Permeation Chromatography techniques, electrical characterization and device fabrication results presented in this work.

References

(1) Elsayed, N. M.; Toxicity of Nitrogen Dioxide: An Introduction. *Toxicology* **1994**, *89* , 161–174.

(2) Morrow, P. E.; An Evaluation of Recent NO_x Toxicity Data and an Attempt to Derive an Ambient Air Standard for NO_x by Established Toxicological Procedures. *Environ. Res.* **1975**, *10*, 92-112.

(3) Pandey, S.; Goswami, G. K.; Nanda, K. K. Nanocomposite Based Flexible Ultrasensitive Resistive Gas Sensor for Chemical Reactions Studies. *Sci. Rep.* **2013**. https://doi.org/10.1038/srep02082.

(4) Rout, C. S.; Hegde, M.; Govindaraj, A.; Rao, C. N. R. Ammonia Sensors Based on Metal Oxide Nanostructures. *Nanotechnology* **2007**, *18*, 205504. https://doi.org/10.1088/0957-4484/18/20/205504.

(5) Li, Z.; Li, H.; Wu, Z.; Wang, M.; Luo, J.; Torun, H.; Hu, P.; Yang, C.; Grundmann, M.; Liu, X.; Fu, Y. Advances in Designs and Mechanisms of Semiconducting Metal Oxide Nanostructures for High-Precision Gas Sensors Operated at Room Temperature. *Mater. Horiz.* **2019**, *6*, 470-506.

(6) Zanolli, Z.; Leghrib, R.; Felten, A.; Pireaux, J.-J.; Llobet, E.; Charlier, J.-C. Gas Sensing with Au-Decorated Carbon Nanotubes. *ACS Nano* **2011**, *5*, 4592–4599.

(7) Singh, E.; Meyyappan, M.; Singh Nalwa, H. Flexible Graphene-Based Wearable Gas and Chemical Sensors. *ACS Appl. Mater. Interfaces* **2017**, *9*, 34544–34586.

(8) Li, F.; Peng, H.; Xia, D.; Yang, J.; Yang, K.; Yin, F.; Yuan, W. Highly Sensitive, Selective, and Flexible NO_2 Chemiresistors Based on Multilevel Structured Three-Dimensional Reduced Graphene Oxide Fiber Scaffold Modified with Aminoanthroquinone Moieties and Ag Nanoparticles. *ACS Appl. Mater. Interfaces* **2019,** *11*, 9309-9316.

(9) Hung, C. M.; Le, D. T. T.; Van Hieu, N. On-Chip Growth of Semiconductor Metal Oxide Nanowires for Gas Sensors: A Review. *J. Sci.: Adv. Mater. Dev*. **2017**, *2*, 263-285.

(10) Steinhauer, S.; Brunet, E.; Maier, T.; Mutinati, G. C.; Köck, A.; Freudenberg, O.; Gspan, C.; Grogger, W.; Neuhold, A.; Resel, R. Gas Sensing Properties of Novel CuO Nanowire Devices. *Sens. Actuators B. Chem.* **2013**, *187*, 50-57.

(11) Rella, R.; Serra, A.; Siciliano, P.; Tepore, A.; Valli, L.; Zocco, A. Langmuir−Blodgett Multilayers Based on Copper Phthalocyanine as Gas Sensor Materials: Active Layer−Gas Interaction Model and Conductivity Modulation. *Langmuir* **1997**, *13*,

6562–6567.

(12) Liao, C.; Yan, F. Organic Semiconductors in Organic Thin-Film Transistor-Based Chemical and Biological Sensors. *Polym. Rev.* **2013**, *53*, 352-406.

(13) Zhang, C.; Chen, P.; Hu, W. Organic Field-Effect Transistor-Based Gas Sensors. *Chem. Soc. Rev*. **2015**, *44*, 2087-2107.

(14) Li, H.; Dailey, J.; Kale, T.; Besar, K.; Koehler, K.; E. Katz, H. Sensitive and Selective NO_2 Sensing Based on Alkyl- and Alkylthio-Thiophene Polymer Conductance and Conductance Ratio Changes from Differential Chemical Doping. *ACS Appl. Mater. Interfaces* **2017**, *9*, 20501–20507.

(15) Ryu, G.-S.; Park, K. H.; Park, W.-T.; Kim, Y.-H.; Noh, Y.-Y. High-Performance Diketopyrrolopyrrole-Based Organic Field-Effect Transistors for Flexible Gas Sensors. *Org. Electron.* **2015**, *23*, 76–81.

(16) Nketia-Yawson, B.; Jung, A.-R.; Noh, Y.; Ryu, G.-S.; Dansoa Tabi, G.; Lee, K.-K.; Kim, B.; Noh, Y.-Y. Highly Sensitive Flexible NH_3 Sensors Based on Printed Organic Transistors with Fluorinated Conjugated Polymers. *ACS Appl. Mater. Interfaces* **2017**, *9*, 7322–7330.

(17) Hoon Yu, S.; Cho, J.; Min Sim, K.; Un Ha, J.; Sung Chung, D. Morphology-Driven High-Performance Polymer Transistor-Based Ammonia Gas Sensor. *ACS Appl. Mater. Interfaces* **2016**, *8* , 6570–6576.

(18) Lu, C. F.; Shih, C. W.; Chen, C. A.; Chin, A.; Su, W. F. Tuning the Morphology of Isoindigo Donor–Acceptor Polymer Film for High Sensitivity Ammonia Sensor. *Adv. Funct. Mater.* **2018**, *28***,** 1803145. https://doi.org/10.1002/adfm.201803145.

(19) Yang, Y.; Zhang, G.; Luo, H.; Yao, J.; Liu, Z.; Zhang, D. Highly Sensitive Thin-Film Field-Effect Transistor Sensor for Ammonia with the DPP-Bithiophene Conjugated Polymer Entailing Thermally Cleavable Tert-Butoxy Groups in the Side Chains. *ACS Appl. Mater. Interfaces* **2015**, *8*, 3635–3643.

(20) Wang, Z.; Huang, L.; Zhu, X.; Zhou, X.; Chi, L. An Ultrasensitive Organic Semiconductor NO_2 Sensor Based on Crystalline TIPS-Pentacene Films. *Adv. Mater.* **2017**, *29,* 1703192. https://doi.org/10.1002/adma.201703192.

(21) Shao, B.; Liu, Y.; Zhuang, X.; Hou, S.; Han, S.; Yu, X.; Yu, J. Crystallinity and Grain Boundary Control of TIPS-pentacene in Organic Thin-film Transistors for the Ultra-high Sensitive Detection of NO_2. *J. Mater. Chem.* C **2019**, *7*, 10196-10202.

(22) Zhuang, X.; Han, X.; Huai, B.; Shi, W.; Yu, J. Sub-ppm and High Response Organic Thin-

Film Transistor NO_2 Sensor Based on Nanofibrillar Structured TIPS-Pentacene. *Sensor Actuat. B. Chem.* **2019**, *279*, 238-244.

(23) Lee, J. H.; Seo, Y.; Park, Y. D.; Anthony, J. E.; Kwak, D. H.; Lim, J. A.; Ko, S.; Jang, H. W.; Cho, K.; Lee, W. H. Effect of Crystallization Modes in TIPS-Pentacene/Insulating Polymer Blends on the Gas Sensing Properties of Organic Field-Effect Transistors. *Sci. Rep.* **2019***, 9*. https://doi.org/10.1038/s41598-018-36652-1.

(24) Bai, S.; Guo, J.; Sun, J.; Tang, P.; Chen, A.; Luo, R.; Li, D. Enhancement of NO_2-Sensing Performance at Room Temperature by Graphene-Modified Polythiophene. *Ind. Eng. Chem. Res.* **2016**, *55*, 5788–5794.

(25) Feng, L.; Tang, W.; Zhao, J.; Yang, R.; Hu, W.; Li, Q.; Wang, R.; Guo, X. Unencapsulated Air-Stable Organic Field Effect Transistor by All Solution Processes for Low Power Vapor Sensing. *Sci. Rep.* **2016**, *6*, 20671. https://doi.org/10.1038/srep20671.

(26) Mori, T.; Kikuzawa, Y.; Noda, K. Improving Baseline Stability of Gas Sensors Based on Organic Field-Effect Transistors by Monitoring Carrier Mobility. *Proc. IEEE Sens.* **2011**. https://doi.org/10.1109/ICSENS.2011.6126923.

(27) Mathijssen, S. G. J.; Cölle, M.; Gomes, H.; Smits, E. C. P.; De Boer, B.; McCulloch, I.; Bobbert, P. A.; De Leeuw, D. M. Dynamics of Threshold Voltage Shifts in Organic and Amorphous Silicon Field-Effect Transistors. *Adv. Mater.* **2007**, *19*, 2785-2789.

(28) Lee, B.; Wan, A.; Mastrogiovanni, D.; Anthony, J. E.; Garfunkel, E.; Podzorov, V. Origin of the Bias Stress Instability in Single-Crystal Organic Field-Effect Transistors. *Phys. Rev. B* **2010,** *82***,** 085302. https://doi.org/10.1103/PhysRevB.82.085302.

(29) Weu, A.; Kress, J. A.; Paulus, F.; Becker-Koch, D.; Lami, V.; Bakulin, A. A.; Vaynzof, Y. Oxygen-Induced Doping as a Degradation Mechanism in Highly Efficient Organic Solar Cells. *ACS Appl. Energy Mater.* **2019**, 2, 1943-1950.

(30) Mun, S.; Park, Y.; Lee, Y. E. K.; Sung, M. M. Highly Sensitive Ammonia Gas Sensor Based on Single-Crystal Poly(3-Hexylthiophene) (P3HT) Organic Field Effect Transistor. *Langmuir* **2017,** *33***,** 13554-13560.

(31) Xie, T.; Xie, G.; Du, H.; Zhou, Y.; Xie, F.; Jiang, Y.; Tai, H. The Fabrication and Optimization of Thin-Film Transistors Based on Poly(3-Hexylthiophene) Films for Nitrogen Dioxide Detection. *IEEE Sens. J.* **2016,** *16*, 1865-1871. https://doi.org/10.1109/JSEN.2015.2480998.

(32) Yang, J.; Xie, G. Z.; Su, Y. J.; Zhang, Q. P.; Du, H. F.; Tai, H. L.; Du, X. S.; Jiang, Y. D. Flexible Organic Thin-Film Transistors Based on Poly(3-Hexylthiophene) Films for

Nitrogen Dioxide Detection. *Sci. China Technol. Sci.* **2018**, *61*, 1696-1704.

(33) Nguyen, K. V.; Payne, M. M.; Anthony, J. E.; Lee, J. H.; Song, E.; Kang, B.; Cho, K.; Lee, W. H. Grain Boundary Induced Bias Instability in Soluble Acene-Based Thin-Film Transistors. *Sci. Rep.* **2016**, *6*, 33224. https://doi.org/10.1038/srep33224.

(34) Veres, J.; Ogier, S.; Lloyd, G.; De Leeuw, D. Gate Insulators in Organic Field-Effect Transistors. *Chem. Mater.* **2004**, *16*, 4543-4555.

(35) Fan, C.-L.; Lin, Y.-Z.; Huang, C.-H. Combined Scheme of UV/Ozone and HMDS Treatment on a Gate Insulator for Performance Improvement of a Low-Temperature-Processed Bottom-Contact OTFT. *Semicond. Sci. Technol.* **2011**, *26*, 045006. https://doi.org/10.1088/0268-1242/26/4/045006.

(36) Louis, B.; Caubergh, S.; Larsson, P. O.; Tian, Y.; Scheblykin, I. G. Light and Oxygen Induce Chain Scission of Conjugated Polymers in Solution. *Phys. Chem. Chem. Phys.* **2018**, *20*, 1829-1837.

(37) Alem, S.; Wakim, S.; Lu, J.; Robertson, G.; Ding, J.; Tao, Y. Degradation Mechanism of Benzodithiophene-Based Conjugated Polymers When Exposed to Light in Air. *ACS Appl. Mater. Interfaces* **2012**, *4*, 2993-2998.

(38) Yu, S.-Y.; Tung, T.-W.; Yang, H.-Y.; Chen, G.-Y.; Shih, C.-C.; Lee, Y.-C.; Chen, C.-C.; Zan, H.-W.; Meng, H.-F.; Lu, C.-J.; Wang, C.-L.; Jian, W.-B.; Soppera, O. A Versatile Method to Enhance the Operational Current of Air-Stable Organic Gas Sensor for Monitoring of Breath Ammonia in Hemodialysis Patients. *ACS Sens.* **2019**, *4*, 1023–1031.

(39) Sizov, A. S.; A. Trul, A.; Chekusova, V.; V. Borshchev, O.; A. Vasiliev, A.; V. Agina, E.; A. Ponomarenko, S. Highly Sensitive Air-Stable Easily Processable Gas Sensors Based on Langmuir–Schaefer Monolayer Organic Field-Effect Transistors for Multiparametric H_2S and NH_3 Real-Time Detection. *ACS Appl. Mater. Interfaces* **2018**, *10*, 43831–43841.

(40) Levi, Z. U.; Tilley, T. D. Synthesis and Electronic Properties of Extended, Fused-Ring Aromatic Systems Containing Multiple Pentalene Units. *J. Am. Chem. Soc.* **2010**, *132*, 11012-11014. https://doi.org/10.1021/ja1043159.

(41) Rahmanudin, A.; Yao, L.; Sivula, K. Conjugation Break Spacers and Flexible Linkers as Tools to Engineer the Properties of Semiconducting Polymers. *Polym. J*. **2018**, *50*, 725-736.

(42) Liu, S. Y.; Shi, M. M.; Huang, J. C.; Jin, Z. N.; Hu, X. L.; Pan, J. Y.; Li, H. Y.; Jen, A. K. Y.;

Chen, H. Z. C-H Activation: Making Diketopyrrolopyrrole Derivatives Easily Accessible. *J. Mater. Chem. A* **2013**, *1*, 2795-2805.

(43) Li, S.; Liu, W.; Shi, M.; Mai, J.; Lau, T. K.; Wan, J.; Lu, X.; Li, C. Z.; Chen, H. A Spirobifluorene and Diketopyrrolopyrrole Moieties Based Non-Fullerene Acceptor for Efficient and Thermally Stable Polymer Solar Cells with High Open-Circuit Voltage. *Energy Environ. Sci.* **2016**, *9*, 604-610.

(44) González-Rosende, M. E.; Castillo, E.; Jennings, W. B.; Malone, J. F. Stereodynamics and Edge-to-Face CH-π Aromatic Interactions in Imino Compounds Containing Heterocyclic Rings. *Org. Biomol. Chem.* **2017**, *15*, 1484-1494.

(45) Chen, S.; Sun, B.; Hong, W.; Yan, Z.; Aziz, H.; Meng, Y.; Hollinger, J.; Seferos, D. S.; Li, Y. Impact of N-Substitution of a Carbazole Unit on Molecular Packing and Charge Transport of DPP-Carbazole Copolymers. *J. Mater. Chem. C* **2014**, *2*, 1683-1690.

(46) White, R. P.; Lipson, J. E. G. Polymer Free Volume and its Connection to the Glass Transition. *Macromolecules* **2016**, *49*, 3987-4007.

(47) Thran, A.; Kroll, C.; Faupel, F. Correlation between Fractional Free Volume and Diffusivity of Gas Molecules in Glassy Polymers. *J. Polym. Sci. Part B Polym. Phys.* **1999**, *37*, 3344-3358.

(48) Qu, M.; Li, H.; Liu, R.; Zhang, S. L.; Qiu, Z. J. Interaction of Bipolaron with the H2O/O2 Redox Couple Causes Current Hysteresis in Organic Thin-Film Transistors. *Nat. Commun.* **2014**, *5*, 3185. https://doi.org/10.1038/ncomms4185.

(49) Gomes, H. L.; Stallinga, P.; Cölle, M.; De Leeuw, D. M.; Biscarini, F. Electrical Instabilities in Organic Semiconductors Caused by Trapped Supercooled Water. *Appl. Phys. Lett.* **2006**, *88*, 082101. https://doi.org/10.1063/1.2178410.

(50) Un, H. I.; Wang, J. Y.; Pei, J. Recent Efforts in Understanding and Improving the Nonideal Behaviors of Organic Field-Effect Transistors. *Adv. Sci*. **2019**, *6*, 1900375. https://doi.org/10.1002/advs.201900375.

(51) Haneef, H. F.; Zeidell, A. M.; Jurchescu, O. D. Charge Carrier Traps in Organic Semiconductors: A Review on the Underlying Physics and Impact on Electronic Devices. *J. Mater. Chem. C* **2020**, *8*, 759-787..

(52) Amit, I.; Octon, T. J.; Townsend, N. J.; Reale, F.; Wright, C. D.; Mattevi, C.; Craciun, M. F.; Russo, S. Role of Charge Traps in the Performance of Atomically Thin Transistors. *Adv. Mater.* **2017**, *29*, 1605598. https://doi.org/10.1002/adma.201605598.

(53) Gieger,M.; Schwarz, L.; Zschieschang, U.; Manske, D.; Pflaum, J.; Weis, J.; Klauk, H.; Weitz, R.T. Quantitative Analysis of the Density of Trap States in Semiconductors by Electrical Transport Measurements on Low-Voltage Field-Effect Transistors *Phys. Rev. Appl.* **2018**, *10*, 044023. https://doi.org/10.1103/PhysRevB.81.155315.

(54) Corrado, T.; Guo, R. Macromolecular Design Strategies toward Tailoring Free Volume in Glassy Polymers for High Performance Gas Separation Membranes. *Mol. Syst. Des. Eng*. **2020**, *5*, 22-48.

(55) Wagner, J.; Jang, H.-J.; Han, J.; Katz, H. E. Enhanced and Unconventional Responses in Chemiresistive Sensing Devices for Nitrogen Dioxide and Ammonia from Carboxylated Alkylthiophene Polymers. *Mater. Horiz.* **2020**. https://doi.org/10.1039/d0mh00049c.

(56) Li, H.; Dailey, J.; Kale, T.; Besar, K.; Koehler, K.; Katz, H. E. Sensitive and Selective NO_2 Sensing Based on Alkyl- and Alkylthio-Thiophene Polymer Conductance and Conductance Ratio Changes from Differential Chemical Doping. *ACS Appl. Mater. Interfaces* **2017**, *9*, 20501-20507.

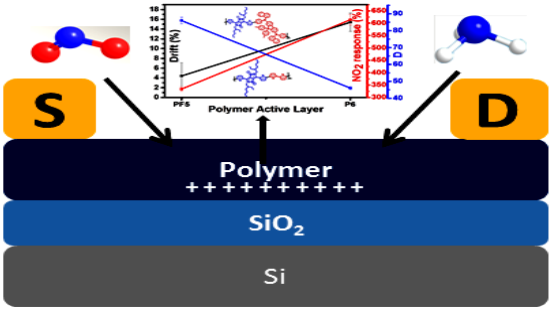

TOC Graphic